

DEV114769 Supplementary Information

Supplementary figure legends

Figure S1: Additional experiments related to Figure 1, Kif5B can be recruited successfully to peroxisomes in myotubes. (A, B) Representative immunoblots of Kif5B and KLC in myotubes treated with siRNA to Kif5B (A) or KLC1 and KLC2 (B); GAPDH serves as a loading control. Levels of kinesin-1 motor complex components are coordinately regulated, as siRNA to either heavy chain or light chain concomitantly reduces both motor components. (C) Myotubes were treated with siRNA to Kif5B to deplete endogenous motors from the cell. Myotubes were also transfected with HA-Kif5B(1-807)-FRB and PEX3-mRFP-FKBP, which targets peroxisomes. Upon ligand addition (1 μ M) labeled peroxisomes exhibit directed motility toward the plus-ends of microtubules and begin to accumulate at the ends of the myotube, indicating successful ligand-mediated motor recruitment. Scale bar: 50 μ m. (D) Movement of individual PEX3-mRFP-FKBP decorated peroxisomes was imaged at higher magnification and time resolution (20 frames per minute) following 60 minutes of ligand treatment. Peroxisomes were tracked manually and tracks are overlaid on the last frame (colored dots). Tracks shown reflect ~90 seconds of imaging. Note that the majority of peroxisomes move toward the end of the myotube where they accumulate. Scale bar: 20 μ m.

Figure S2: Line scan examples and additional controls associated with Figure 2

(A) Line scan analyses corresponding to the examples of Kif5B siRNA-treated myotubes co-expressing FKBP-EGFP-KASH and HA-Kif5B(1-807)-FRB as shown in Fig 2C. All nuclei were independently evaluated for the presence of HA-Kif5B(1-807)-FRB on the

NE by quantitative line scan analysis. A 50-pixel line, beginning in the cytoplasm and centered at the NE, was drawn on the raw Tiff image in the FKBP-EGFP-KASH channel using Fiji (*a,b* top panel, magenta lines). The coordinates of this line were transferred to the HA-Kif5B(1-807)-FRB image and the intensity values along these lines were obtained for both channels. For each line, values were normalized to the mean of the first 15 pixels (cytoplasmic signal). The standard deviation of the first 15 pixels was also determined and nuclei were considered HA⁺ if the normalized fluorescence intensity signal at the midpoint of the 50-pixel line was above 3× the standard deviation (grey shading on line scan graphs). Plus and minus marks indicate the designation of a particular nucleus as HA⁺ or HA⁻ based on the above criteria. (B) Representative image showing normal nuclear distribution and myofibril development in a ligand-treated C2C12 myotube. Nuclei are labeled with Hoechst dye (magenta); α -actinin is in green. (C) Nuclei aggregate at the midline of Kif5B siRNA + ligand treated myotubes expressing FKBP-EGFP-KASH. Nuclei are labeled with Hoechst dye (magenta); EGFP is shown in green. (D) Nuclei aggregate at the midline of Kif5B siRNA + ligand-treated myotubes expressing HA-Kif5B(1-807)-FRB. Nuclei are labeled with Hoechst dye (magenta); HA-Kif5B-FRB is in green. Images in A-C are maximum projections of confocal *z*-sections. Scale bar: 50 μ m. (E) Distribution of nuclei in treated myotubes. Each line on the *y*-axis represents an individual myotube, organized according to length ($N = 50$ -57 myotubes). The ends of the myotube are marked by a dark square; data points represent individual nuclei. (F) Frequency distributions of the distance between adjacent nuclei in treated myotubes (1 μ m bin width; less than 1.5% of the data lies above 105 μ m

so distributions are truncated for clarity). (G) Histogram depicting nuclear position as a percentage of the distance along the myotube length (bin width = 10%).

Figure S3: Additional co-immunoprecipitation experiments associated with Figure 3.

COS7 cells were transfected with EGFP-nesprin 2 (6348-6552) and HA-KLC2 WT or R251D, N287L and R312E mutants. (A) IP of EGFP-nesprin-2, followed by immunoblot analysis using both anti-EGFP and anti-HA antibodies indicates that point mutations in KLC2 reduce binding to EGFP-nesprin-2. (B) The reciprocal IP of HA-KLC2 WT and mutants reveals the same reduction in binding between EGFP-nesprin-2 (6348-6552) and KLC2 R251D, N287L and R312E mutants.

Figure S4: Additional controls associated with Figure 4. (A) COS7 cells were transfected with Myc-Kif5B-Halo and EGFP-KLC2 WT or mutant constructs. IP of EGFP-KLC2, followed by immunoblot analysis using both anti-EGFP and anti-Myc antibodies indicates that point mutations in KLC2 do not prevent binding to Myc-Kif5B-Halo. (B,C) KLC1 immunofluorescence in myotubes treated with Mock siRNA, KLC1 and KLC2 siRNA (B) and KLC1 and KLC2 siRNA + HA-KLC2 WT or R251D, N287L or R312E mutant constructs (C). Images correspond to the myotubes in Figure 4C & D. Only Mock siRNA-treated myotubes show expression of KLC1 in the cytoplasm and on the nuclear envelope. Images are maximum projections of confocal z -sections. Scale bar: 50 μm . (D) COS7 cells were transfected with Myc-Kif5B-Halo, HA-KLC2 WT or mutant constructs along with EGFP or EGFP-MAP7. Immunoprecipitation of EGFP-MAP7, followed by immunoblot analysis using anti-GFP, anti-Myc and anti-HA

antibodies indicates that point mutations in KLC2 do not disrupt the interaction of MAP7 with Kif5B.

Figure S5: Additional data associated with Figure 5. (A) Representative immunoblots of nesprin-1 and nesprin-2 in myotubes treated with siRNA targeted against the 3'UTR of both nesprin-1 and nesprin-2; actin serves as the loading control. Blots were detected with rabbit polyclonal anti-nesprin antibodies generated by Didier Hodzic at Washington University in St Louis, USA. (B) COS7 cells were transfected with EGFP, YFP-RanBP2-KBD WT or mutant (Mut) constructs (Cho et al., 2007) along with HA-KLC WT or TPR mutant constructs. IP of YFP-RanBP2-KBD, followed by immunoblot analysis using anti-GFP and anti-HA antibodies, indicates the WT KBD domain of RanBP2 (previously shown to bind the Kif5B and Kif5C heavy chain) also binds KLC2 and this interaction is disrupted by point mutations in the TPR domain of KLC2. No endogenous Kif5B was detected in these binding assays, suggesting RanBP2 can bind KLC independent of KHC. In support of this, the mutations in the KBD that blocks KHC binding (Cho et al., 2007), do not block binding of RanBP2 KBD to HA-KLC2 WT.

Supplementary materials & methods

Construct Generation

FKBP-EGFP-KASH was generated by PCR using the 2xFKBP12 fragment from PEX3-mRFP-FKBP and then subcloning into the EGFP-nesprin-2 α -KASH vector. Myc-Kif5B-Halo was generated by first inserting the Halo-tag from the pHTC HaloTag CMV-neo vector (Promega) at the C-terminus of pRK5-Myc-Kif5C and then Kif5C was replaced with Kif5B from pRK5-Myc-Kif5B. EGFP-nesprin-2 (6146-6799) and (6348-6552) WD/AA mutants were generated using the QuikChange Lightning Multi Site-Directed Mutagenesis Kit with the mutagenic primer (5'-CCCCCTGGAGGCGGCCACACAGGC3-3'). The mutant fragment was sequenced in its entirety and sub-cloned into EGFP-nesprin-2 (6146-6799) and EGFP-nesprin-2 (6348-6552). Final WD/AA mutagenic constructs were sequenced for accuracy. EGFP-nesprin-2 (6348-6552)-KASH constructs were generated by inserting the PCR product for nesprin-2 (6348-6552)(WT or WD/AA) in frame between EGFP and KASH in the EGFP-nesprin-2 α -KASH vector.

siRNA oligonucleotides

siRNA oligos were directed against mouse Kif5B (NM_008448, EG-ID 16573, 5'-GGAGGAGGCUCAUUUGUUC-3', targets ORF); mouse KLC1 (NM_008450, EG-ID 16593, 5'-GAGUAUGGCGGCUGGUAUA-3', targets ORF); mouse KLC2 (NM_008451, EG-ID 16594, 5'-CUGUAGAAAUAAGACGAU-3', targets 3'UTR); mouse nesprin-1 (NM_022027, 5'-AGUAAGAGGAGAAGGAAUA-3', targets 3'UTR); mouse

nesprin-2 (NM_015180, 5' - UGGCAGAACUAGUUGAUUA-3', targets 3'UTR) were from GE Healthcare Dharmacon.

Figure S1

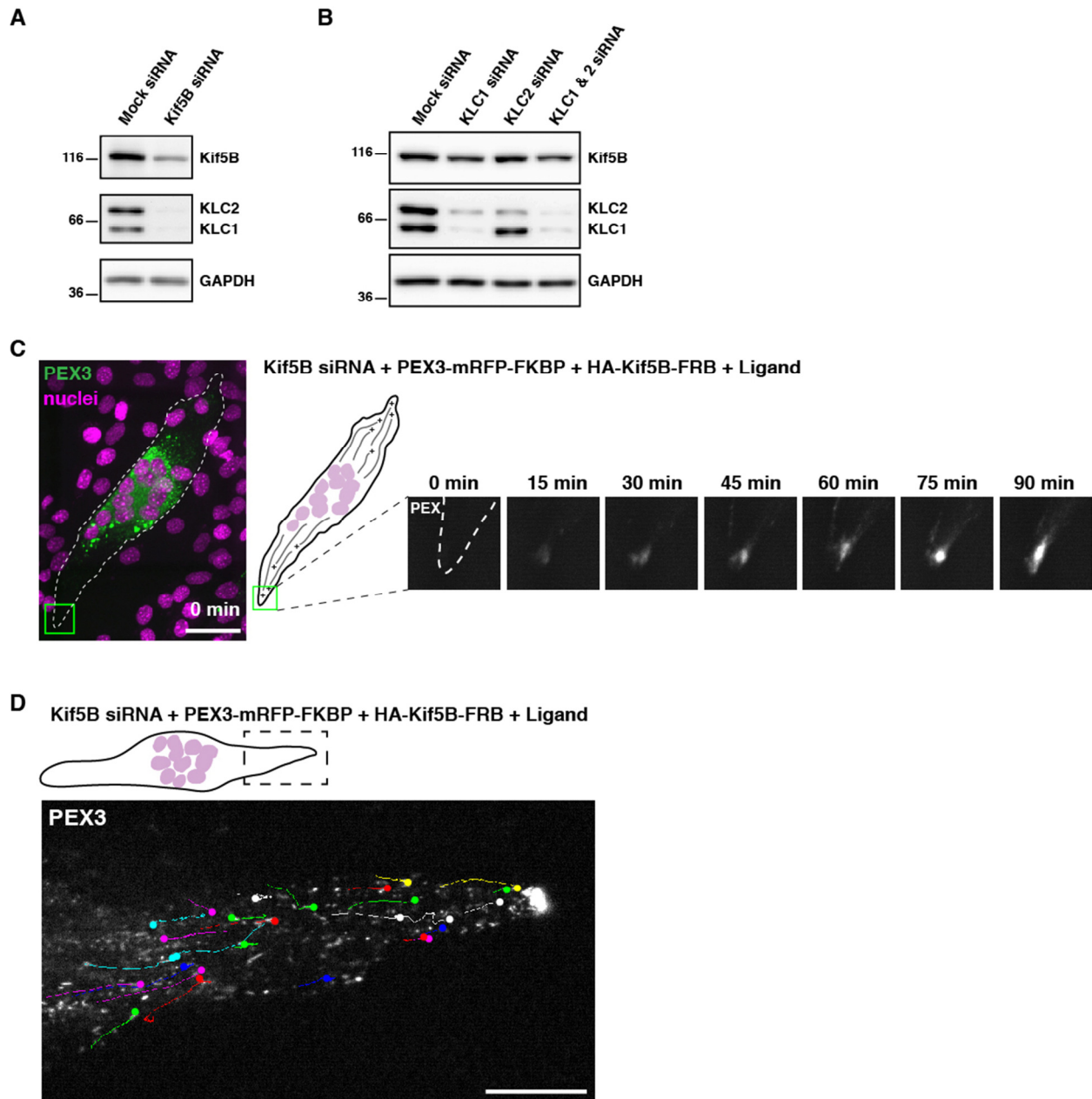


Figure S2

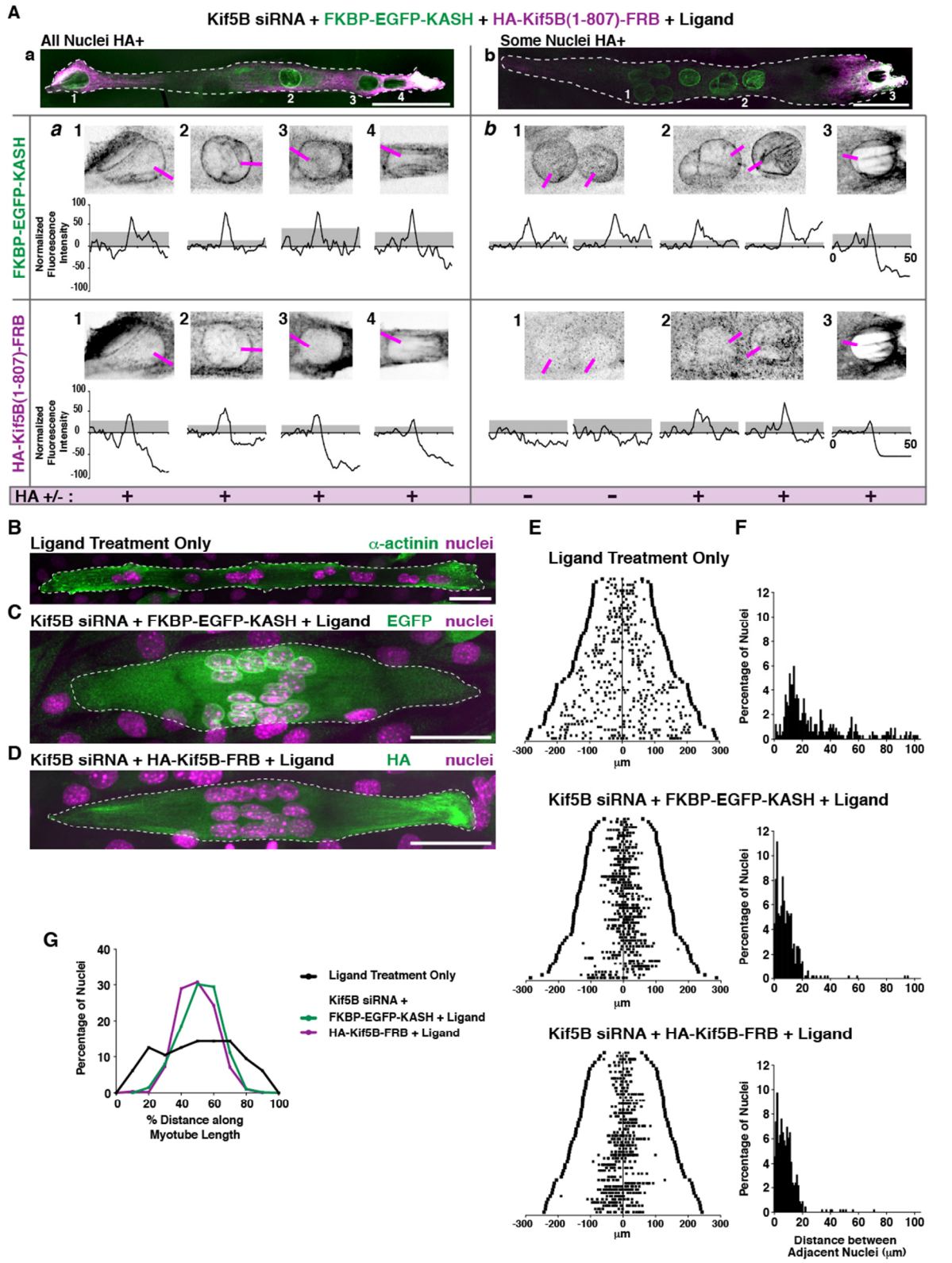


Figure S3

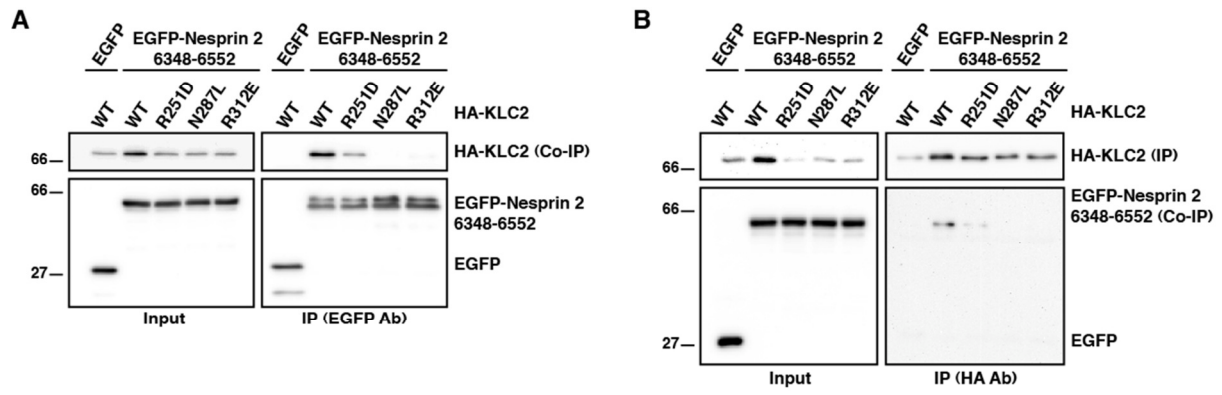


Figure S4

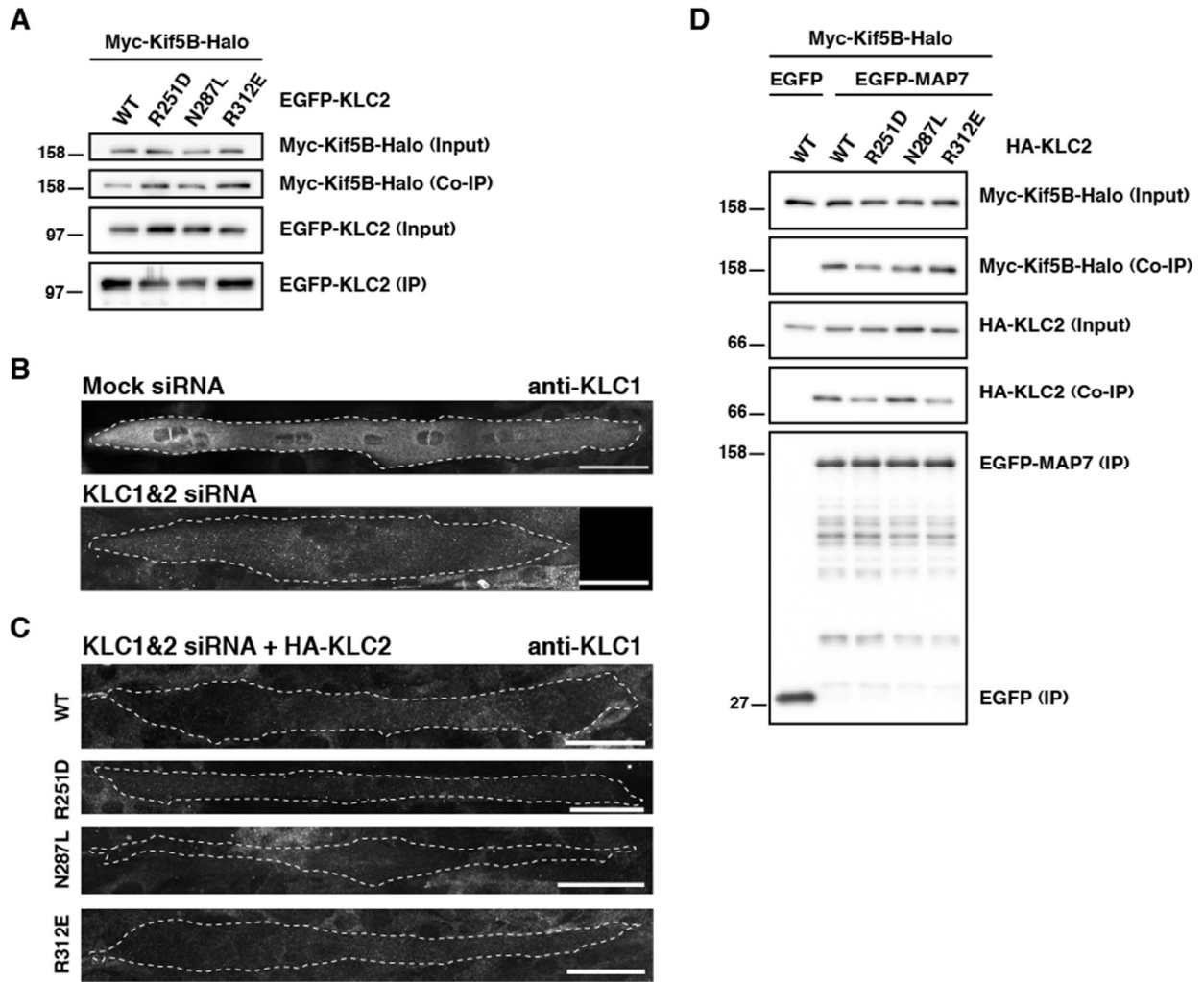


Figure S5

